


Numerical unmixing of weakly and strongly magnetic minerals: examples with synthetic mixtures of magnetite and hematite

Journal Article**Author(s):**

Liu, Pengfei; [Hirt, Ann Marie](#) ; Schüler, Dirk; Uebe, René; Zhu, Peimin; Liu, Tianyou; Zhang, Henglei

Publication date:

2019-04

Permanent link:

<https://doi.org/10.3929/ethz-b-000340130>

Rights / license:

[In Copyright - Non-Commercial Use Permitted](#)

Originally published in:

Geophysical Journal International 217(1), <https://doi.org/10.1093/gji/ggz022>

Numerical unmixing of weakly and strongly magnetic minerals: examples with synthetic mixtures of magnetite and hematite

Pengfei Liu,^{1,2} Ann M. Hirt,² Dirk Schüler,³ Rene Uebe,³ Peimin Zhu,¹ Tianyou Liu¹ and Henglei Zhang¹

¹Hubei Subsurface Multi-scale Imaging Key Laboratory, Institute of Geophysics and Geomatics, China University of Geosciences, Wuhan 430074, China

²Institute of Geophysics, ETH Zürich, Sonneggstrasse 5, CH-8092 Zürich, Switzerland. E-mail: ann.hirt@erdw.ethz.ch-N.B.

³Lehrstuhl Mikrobiologie, Universität Bayreuth, Universitätsstrasse 30, D-95477 Bayreuth, Germany

Accepted 2019 January 15. Received 2019 January 9; in original form 2018 May 24

SUMMARY

The characterization of magnetic minerals in rocks often uses methods that measure induced magnetization. When rocks, sediments or soils contain two magnetic phases, in which one has a high saturation magnetization (M_S), for example magnetite, and the other a low M_S , for example hematite, the induced magnetization will be dominated by the stronger phase. An earlier study by Frank and Nowaczyk has shown that even when magnetite makes up <10 wt per cent of the ferromagnetic content, it will mask hematite. This makes identification of phases with low M_S difficult to identify. We conduct a systematic study of synthetic mixtures of single domain magnetite and hematite with a broad spectrum of particle size, using hysteresis properties, acquisition of isothermal remanent magnetization (IRM) and first-order reversal curve distributions (FORC). Hysteresis parameters and FORC distributions do not vary significantly from the pure magnetite sample for hematite concentrations ≤ 90 wt per cent. IRM is not saturated for hematite concentration of 30 wt per cent or higher. Principle component analysis (PCA) of the processed FORCs, detects the presence of hematite for concentrations 70 wt per cent at the very least. Our results illustrate the difficulty in identifying hematite when it is found together with magnetite. IRM acquisition is the most sensitive method for identifying hematite when it occurs together with magnetite.

Key words: Magnetic properties; Magnetic mineralogy and petrology; Rock and mineral magnetism; Statistical methods.

1 INTRODUCTION

Magnetite and hematite are the most common ferromagnetic minerals that are found in crustal rocks. The ability to identify these two minerals in a rock or sediment, based on their magnetic properties, is important in both palaeomagnetic and environmental studies. The properties that are used to distinguish the two phases include their hysteresis properties, for example saturation magnetization (M_S), remanent magnetization (M_{RS}), coercive force (B_C) or remanent coercive force (B_{CR}), Curie/Néel temperature and low temperature transitions, for example Verwey transition for magnetite or Morin transition for hematite. Although determination of Curie or Néel temperature leads to a unique identification, it is not always possible to heat a material, particularly for sediments and soils. More commonly, measurement of induced magnetization is used to identify ferromagnetic minerals in rocks and sediments; however, similar hysteresis parameters can reflect different combination of ferromagnetic minerals (e.g. Parry 1982; Roberts *et al.* 1995; Dunlop 2002; Muxworthy *et al.* 2003; Carvallo & Muxworthy 2006). For

this reason, several methods have been developed to aid in separating contributions from different ferromagnetic phases. Due to the difference in coercivity between the two minerals, acquisition of isothermal remanent magnetization (IRM, Robertson & France 1994; Kruiver *et al.* 2001), S-ratio (Bloemendal *et al.* 1988; King & Channell 1991), or hard-IRM (HIRM, Thompson & Oldfield 1986) are often used in identification of the two minerals. Liu *et al.* (2002) proposed a method for separating weak magnetic signal (e.g. hematite/goethite) from a strong ferrimagnetic background (e.g. magnetite/maghemite) by applying alternatives field (AF) demagnetization of an acquired IRM. Lagroix & Guyodo (2017) describe a semi-quantitative method for the decomposition of mixtures of different ferromagnetic phases by employing a measurement protocol for low temperature susceptometers. They were able to identify the presence of both low and high coercivity minerals in loess and palaeosols samples.

Frank & Nowaczyk (2008) carried out a systematic rock magnetic study on artificial mixtures of magnetite and hematite to investigate which magnetic parameters best delineate the two phases. They

Table 1. Magnetite and hematite mixing series and associated magnetic parameters.

Samples	Hematite		B_{CR} (mT)	M_{RS} (Am ² kg ⁻¹)	M_S (Am ² kg ⁻¹)	S-ratio	HIRM
	(wt per cent)	B_C (mT)					
LMU-30	0	16.6	21.6	28.99	71.32	1.00	0.058
Mt_Hm_10	10	16.7	21.5	26.35	64.76	1.00	0.025
Mt_Hm_22	22	16.3	21.5	22.26	56.34	1.00	0.032
Mt_Hm_31	31	16.5	21.5	20.09	50.51	1.00	0.026
Mt_Hm_40	40	16.4	21.3	17.73	43.91	1.00	0.033
Mt_Hm_50	50	16.6	21.3	14.77	36.40	0.99	0.040
Mt_Hm_61	61	16.5	21.4	11.66	29.03	0.99	0.039
Mt_Hm_70	70	16.2	21.4	8.737	22.18	0.98	0.048
Mt_Hm_80	80	16.0	20.9	5.969	14.83	0.98	0.059
Mt_Hm_85	85	15.4	20.4	4.439	11.34	0.96	0.058
Mt_Hm_90	90	14.0	19.1	2.896	7.722	0.96	0.065
Mt_Hm_95	95	12.1	17.0	1.331	3.737	0.93	0.055
Hematite	100	106.6	345.5	0.141	0.493	0.21	0.079

showed that hematite concentrations less than 90–95 per cent are largely not detectable by coercivity-based parameters, for example B_C , B_{CR} and median destructive field of ARM (MDF_{ARM}) when magnetite is present. Parameters, involving remanent magnetization rather than induced magnetization, for example S-ratio or HIRM, delineate hematite at concentrations of 90 wt per cent or higher.

A number of other studies have investigated synthetic and natural mixtures of ferromagnetic minerals with either differences in grain size or composition in order to evaluate the methods applied for extracting this information (Heslop *et al.* 2002; Egli 2004; Dunlop & Carter-Stiglitz 2006; Heslop & Dillon 2007; Lascu *et al.* 2010; Heslop & Roberts 2012a, 2012b; Heslop 2015), but most studies provided no information on the absolute concentrations of the different phases. Pike *et al.* (1999, 2001) and Roberts *et al.* (2000) have demonstrated a powerful method, known as the first-order reversal curve (FORC) analysis, to discriminate different magnetic components in geological samples. A FORC diagram is established by measuring a series of partial hysteresis curves, termed FORCs (Mayergoyz 1986), and distinguishes the coercivity spectrum and spectrum of interaction fields in a material. Muxworthy *et al.* (2005) assessed the ability of FORC technique to reveal mixtures of magnetic minerals with different coercivities. Their results indicated that the FORC method is very applicable in discriminating between hard and soft magnetic minerals as long as the concentration of the phase with higher M_S is not too large. Carvallo & Muxworthy (2006) demonstrated that FORC analysis on mixtures of magnetite and hematite with single domain particle size could only detect hematite when its concentration was >88 wt per cent. Harrison & Feinberg (2008) have proposed an improved algorithm for processing the FORCs into a FORC diagram, which shows coercivity plotted against interaction field. The FORC method has been further developed, e.g. extraction the central ridge of FORC distribution, which further aids in distinguishing different magnetic components (Egli *et al.* 2010; Egli 2013; Ludwig *et al.* 2013; Heslop *et al.* 2014; Lascu *et al.* 2015).

In this study, we return to the problem of identifying mixtures of magnetite, a low coercivity phase, with hematite, a high coercivity phase, and evaluate which magnetic parameters and measurement techniques best decompose the two phases. A series of synthetic mixtures made up of magnetite with varying concentrations of hematite were prepared. We focus specifically on using the direct-current demagnetization (DCD) curves and FORC analysis to evaluate the ability of these methods to better distinguish hematite when it occurs together with magnetite. In addition, the

FORC results are further evaluated using principal component analysis (PCA), which is described in Lascu *et al.* (2015). Their method performs PCA on the part of the FORC space that carries a significant magnetic signature in a material. The method evaluates the variability as a linear combination of significant component, which arises only from variability within the data set, and provides a means for quantitative unmixing of magnetic minerals. This study addresses the question if PCA analysis can resolve the presence of high coercivity hematite in the presence of magnetite.

2 SAMPLES AND METHODS

2.1 Samples

The end-members for the mixtures consisted of magnetosomes of biogenic magnetite (LMU-30), isolated from the magnetotactic bacterium *Magnetospirillum gryphiswaldense* as described previously (Lohße *et al.* 2016) with a mean particles size of 37 nm, and a commercial synthetic hematite powder with >99.9 per cent purity and sub- μ m size (Hem21, Merck). Note that the LMU-30 is made up of magnetosomes and not chains, although some self-assembly may occur. The magnetic properties were first defined for the end-member samples, and subsequently hematite was added to the magnetite sample. LMU-30 was pipetted from a colloid into a small quartz glass cylinder with 5 mm diameter (3 mm inner diameter) and 11 mm length that was sealed on one end with epoxy. This was then placed on a magnet and excess water was pipetted from the mixture. This process was repeated several times and the sample was left to dry in a refrigerator for 24 hr. The mass of magnetite was 1800 μ g. Initially 200 μ g of hematite was added to the holder with magnetite sample and a small piece of sterile cotton was pressed downwards to fix the particles before measurement. Subsequently, 10 further incremental additions of hematite were made, following the same procedure. This yielded 11 sets of data with hematite concentration between 10.0 and 95.0 wt per cent hematite. The sample name reflects the wt per cent of hematite in the sample, for example Mt_Hm_10 is 10 wt per cent hematite (Table 1).

2.2 Methods

Curie/Néel temperature was defined on the end-members using thermomagnetic measurements on an Agico Multi-Function Kappabridge (MFK1-FA), which has a sensitivity of 2×10^{-8} (SI) and

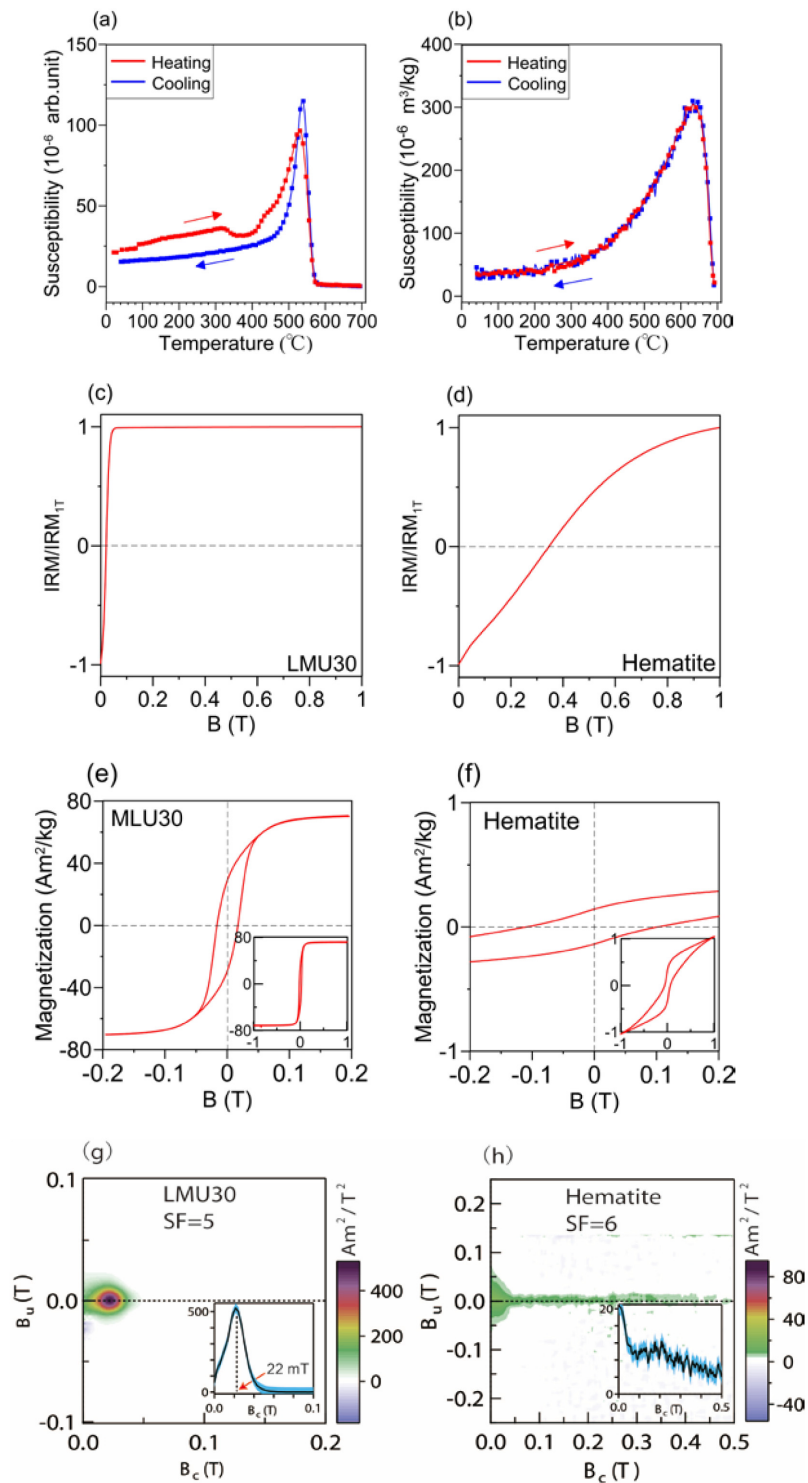


Figure 1. Magnetic characterization of end-members magnetite sample (LMU-30) and hematite sample (HEM21). Panels (a) and (b) thermomagnetic curves; (c) and (d) IRM acquisition; (e) and (f) hysteresis loops; (g) and (h) FORC diagrams. Note that (g) has been truncated to 200 mT and (h) have been truncated to 500 mT to better show the FORC distribution.

an accuracy of ± 0.1 per cent within one range. The magnetite samples were heated in Ar atmosphere, whereas hematite was heated in air, with a heating rate of $11 \text{ }^\circ\text{C min}^{-1}$. Curie, respectively Néel temperature, was defined from an average of the second derivative of the heating and cooling curves. Hysteresis loops, acquisition of

IRM, and FORC analysis were made using a Princeton Measurements Corporation (PMC) vibrating sample magnetometer (VSM), which had a sensitivity $4 \times 10^{-9} \text{ Am}^2$ (standard deviation) for our measurement protocol. Hysteresis was measured using 100 ms averaging time, and a multisegment measurement scheme with 0.5

mT steps in fields $\leq \pm 98$ mT, 2 mT between ± 100 and ± 200 mT and 5 mT in fields between ± 205 and ± 1000 mT. DCD curves or backfield demagnetization was used for IRM acquisition. Samples were first magnetized in 1000 mT in a positive direction and then incrementally remagnetized and in the opposite direction, using 6 mT field increment and 100 ms averaging time. *S*-ratio is defined as IRM 150 mT divided by the absolute change from the IRM between 0 mT and a backfield of 1000 mT. HIRM is defined as 0.5 multiplied IRM acquired in a backfield of 1000 mT minus the IRM acquired in a backfield of 300 mT (King & Channell 1991). FORC measurements were made using a saturating field of 1000 mT, a measurement increment of 5.41 mT, B_{Cmax} of 700 mT, B_U of ± 100 mT and 180 individual FORCs. All measurements were made at the Laboratory of Natural Magnetism, ETH Zurich, Switzerland. FORC data were processed using FORCinel (v3.03, Harrison & Feinberg 2008; Lascu *et al.* 2015) and principal component analysis (PCA) of the FORC data were made with FORCinel (v3.05, Harrison *et al.* 2018). A smoothing factor of $SF = 6$ was used to process all FORC diagrams except for end-member LMU-30, in which $SF = 5$ was used.

3 RESULTS

Table 1 summarizes the magnetic parameters for the end-members and mixed samples.

3.1 End-members

The purity of the magnetite and hematite was checked by their Curie and Néel temperature, respectively. LMU-30 shows a gradual increase in susceptibility during heating with a large increase due to a Hopkinson effect between 400 and 537 °C (Fig. 1a). The Curie temperature was defined at 554 °C, which is slightly below what one would expect for stoichiometric magnetite, 580 °C (Dunlop & Özdemir 1997). There is an indication for some maghemization in the heating curve as indicated in the thermomagnetic curve by the decrease in susceptibility between 320 and 355 °C. The hematite powder also shows a large increase in susceptibility starting around 300 °C with an abrupt drop starting at 632 °C (Fig. 1b). The Néel temperature is 671 °C, which is close to the reference value of 675 °C given in Dunlop & Özdemir (1997).

The DCD curve shows that magnetite is saturated by 60 mT and has a remanent coercive force, B_{CR} of 21.6 mT. Hematite shows an initial concave curve with a steeper slope between 12 and 50 mT and slower acquisition at higher fields. The IRM is not saturated by 1000 mT and B_{CR} is 345.5 mT (Figs 1c and d). The low coercivity contribution may be due to the presence of larger particle sizes (Heslop 2015) or measurement within the basal plane of some hematite crystals because no magnetite and/or maghemite was detected in the thermomagnetic measurements. Hysteresis loops for end-members are shown in Figs 1(e) and (f). The coercive force, B_C , for LMU-30 is 16.6 and 106.6 mT for hematite. LMU-30 is rapidly magnetized in small fields and is saturated by 150 mT with a saturation magnetization of 70 $\text{Am}^2 \text{kg}^{-1}$ (Fig. 1e), which may suggest some degree of surface oxidation to maghemite. Hematite is still not saturated at the maximum applied field of 1 T (Fig. 1f). It shows a more rapid increase in the initial fields up to 50 mT and then a more gradual acquisition.

The FORC distribution for LMU-30, as shown in Fig. 1(g), reflects single domain behaviour with peak coercivity of 22 mT and a relatively limited distribution in interaction field, typical for what is seen for a sample on non-interacting SD magnetite (e.g. Kumari

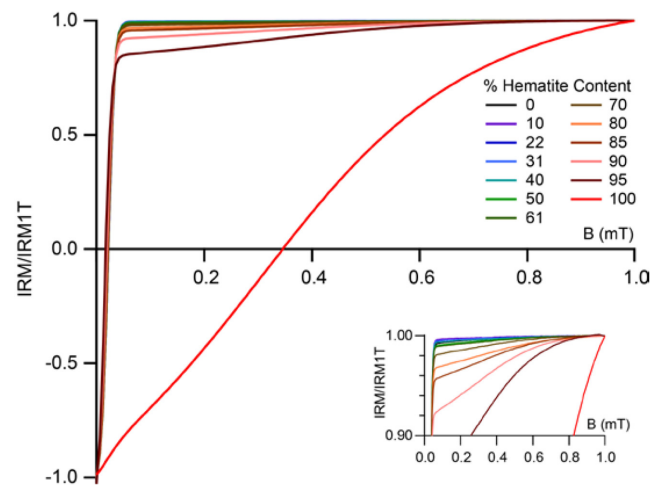


Figure 2. Direct current demagnetization curves.

et al. 2014). The FORC distribution for hematite shows a broad coercivity distribution with two peak coercivities (Fig. 1h). The lower peak is around 10 mT and may represent coarse grains or particles whose crystallographic basal plane is in the field direction (Martin-Hernandez & Hirt 2013). The higher coercivity peak is around 200 mT. In summary, the characteristics of thermomagnetic curve, the DCD curve and FORC distribution indicates that LMU-30 is pure SD and hematite is pure hematite, but with a broad coercivity distribution.

3.2 Mixtures

3.2.1 DCD

DCD curves are saturated by approximately 60 mT for the mixtures of magnetite and hematite up to 30 wt per cent (Fig. 2). The non-saturated part of the IRM is ≤ 1 per cent for samples between 30 and 61 wt per cent hematite. By 70 wt per cent hematite, it is clear that the IRM is not saturated, and the non-saturated contribution increases with increasing hematite content. *S*-ratio, however, remains above 0.95 for all mixtures until 95 wt per cent hematite, similar to what was found by Frank & Nowaczyk (2008).

3.2.2 Hysteresis loops

The results of major hysteresis loops are shown in Figs 3 and S1. Loops are closed by 100 mT for concentrations up to 85 wt per cent hematite. M_S , M_{RS} and IRM_{1T} show a steady decrease with increasing hematite concentration, however, the magnetization ratio (M_{RS}/M_S) does not significantly vary until 80 per cent hematite (Fig. S2). B_C and B_{CR} remain relatively constant with only a decrease above 80 wt per cent hematite. From the bulk data, it is difficult to discriminate and identify changes in hematite concentration in the mixtures from the shape of the hysteresis loops. The changes, however, are reflected better in plotting M_{RS}/M_S against B_{CR}/B_C in a Day-Dunlop plot (Fig. 4). LMU-30 has a high magnetization ratio but the magnetization ratio decreases and the coercivity ratio increases with the initial addition of hematite. This trend continues until 95 wt per cent hematite, but a noticeable difference is only found for concentrations > 90 wt per cent. Note that the pure hematite plots with a low magnetization ratio and high coercivity ratio.

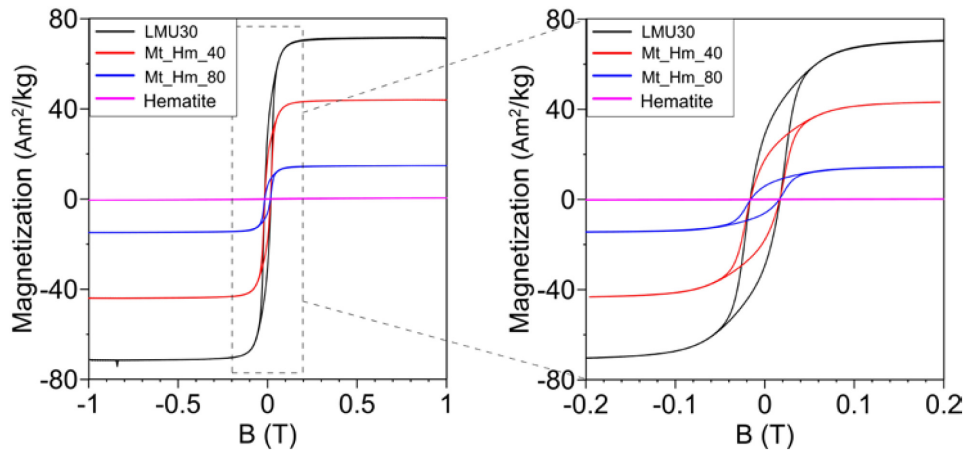


Figure 3. Comparison of hysteresis loops for selected magnetite/hematite mixtures.

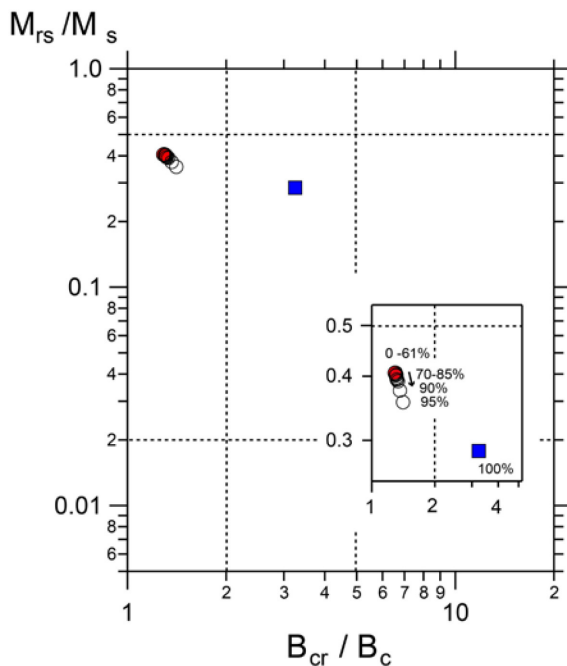


Figure 4. Day-Dunlop plot for all magnetite/hematite mixtures. Inset show more detail and percentages indicate the per cent hematite concentration.

3.2.3 FORC

The detailed results from FORC analysis are shown for selected samples in Fig. 5. The FORC distributions are similar in the mixtures before reaching 80 wt per cent hematite. Comparing Figs 5(a)–(f), a concentration of hematite around 90 wt per cent is needed before visibly influencing the FORC distribution. The FORC distribution is confined along $B_U = 0$, but with small differences in spread along B_C . The density spectrum at $B_C = 0$ shows a slight increase in comparison to LMU 30 with the addition of hematite (Figs 1g, 5a–h, S3).

Although the FORC distribution shows some different characteristics depending on the hematite concentration, it is still difficult to depict a general trend in the change. To further study the characteristic hysteresis properties of the mixtures, we analysed the FORC data using PCA with FORCinel (v3.05) (Harrison *et al.* 2018). Note that the data resolution for PCA grid is 5.41 mT. The variability in the mixtures is mainly accounted for by PC1 (Fig. 6), i.e. magnetite,

which explains 70.0 per cent contribution of the data variability, and PC2, that is the hematite component accounts for the remaining 30 per cent. The low contribution of the hematite end-member to the variability illustrates one problem with detecting hematite in FORC analysis, which is discussed below. The FORC distribution should be described by two end-members (Fig. 6). The end-members (EMs) can be related to single domain magnetite (EM1), and a high and low coercivity hematite (EM2). The PC1 score remains the same for the pure magnetite and mixtures up to 85 wt per cent hematite. Only by 90 wt per cent hematite is there a distinct difference in the PC1 score. The PCA analysis described in Harrison *et al.* (2018) generates FORCs for the end-members as shown in Fig. 6. The PCA program is able to produce a FORC diagram for EM1, the magnetite end-member, that captures all features of the FORC for LMU-30. Although the FORC for EM2 captures the high coercivity ridge, it is unrealistic and cannot reproduce the low coercivity portion of the diagram. This point is discussed below.

4 DISCUSSION

The magnetite/hematite mixture series in this study show a similar change in bulk hysteresis properties with respect to hematite concentration as seen in Frank & Nowaczyk (2008). B_C only starts to change noticeably at 90 wt per cent hematite, and B_{CR} only changes significantly by 95 wt per cent hematite; therefore, coercivity ratio is also not affected until >90 wt per cent hematite. It should be noted that Frank & Nowaczyk (2008) saw a rise in B_C and B_{CR} above 90 wt per cent hematite, whereas we see a decrease. This difference is related to the low coercivity contribution that is found in the hematite powder, which was used in this study. As stated above the low coercivity component can arise from magnetization along the basal plane or particle size. The coercivity ratio, B_{CR}/B_C , in both our study and Frank & Nowaczyk (2008), increases above 90 wt per cent hematite. Both M_S and M_{RS} show a linear decrease in intensity with increasing hematite concentration, but the magnetization ratio is relatively constant until hematite concentration >90 wt per cent.

Although the S-ratio remains above 0.9 for all mixtures of magnetite and hematite, the DCD curve shows that magnetization is not saturated when the hematite concentration of 30 wt per cent or higher. Although from a statistical point of view M_R , M_{RS} and HIRM are significantly different from one sample mixture to another (Table S1), the question is how to evaluate a measurement value from a

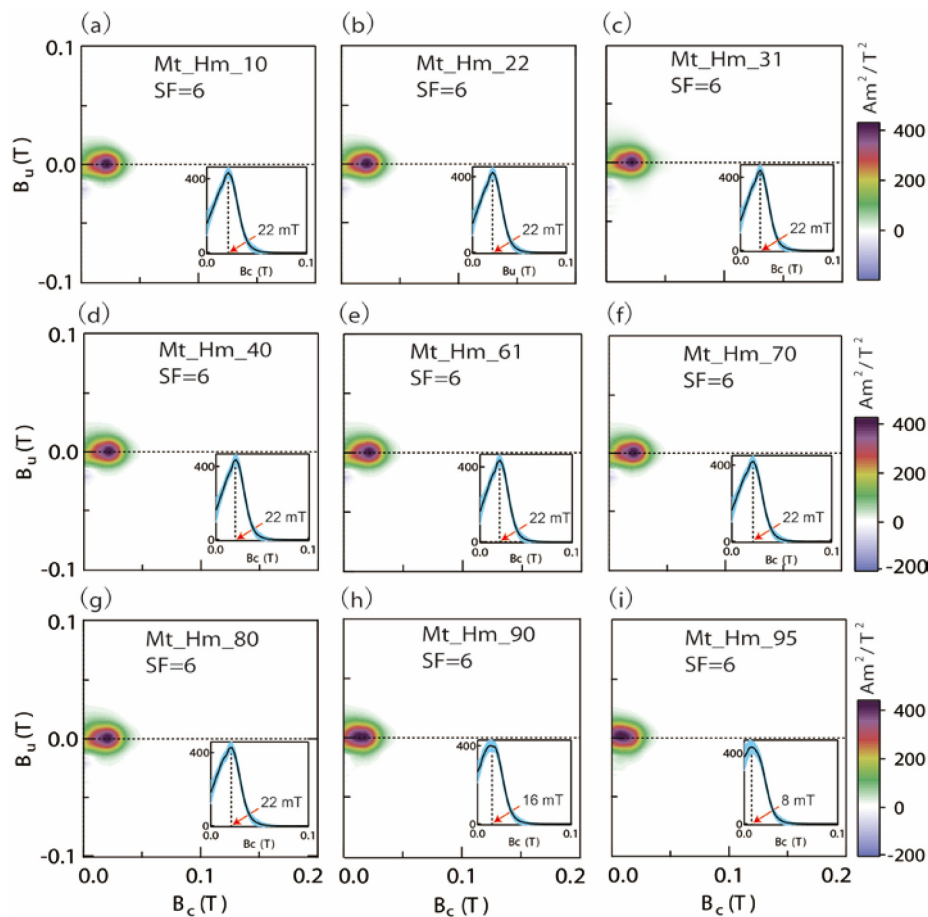


Figure 5. FORC diagrams of selected mixtures. Inset shows the density distribution in Am^2/T^2 as a function of B_c . Note that the FORC diagrams have been truncated to 200 mT to better show the FORC distribution. Intensity scale is the same in all plots.

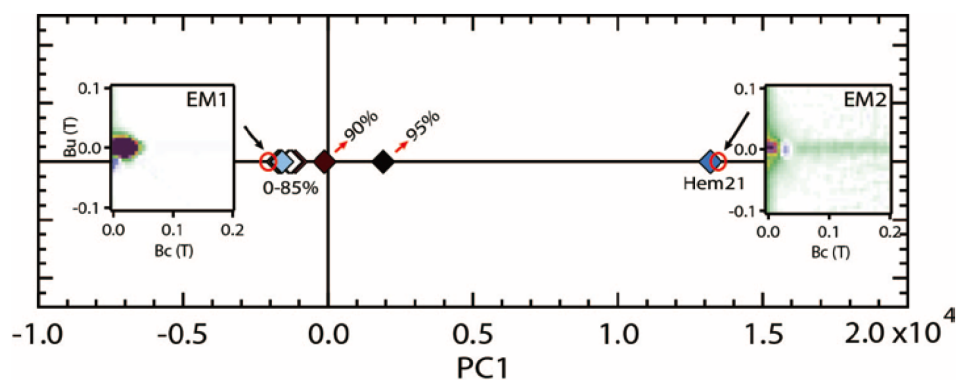


Figure 6. Binary PCA analysis. The resolution for PCA grid is 5.41 mT.

sample in which there is no information on the amount of magnetite versus hematite. Therefore for our sample series the first mixture that is clearly not saturated has 31 wt per cent hematite. From the palaeomagnetic literature many studies would the IRM acquisition curve as having a negligible hematite content. Frank & Nowaczyk (2008) noted that IRM was not saturated for concentrations of 80.1 wt per cent or higher, although their sample for 59.7 wt per cent hematite is not completely saturated. A recent study by Ahmadzadeh *et al.* (2018), who were interested in detecting hematite in commercial powders, also evaluated magnetite mixtures with 90 wt per cent hematite or higher. They measured hysteresis loops, FORCs, and

IRM acquisition, and report that IRM acquisition curves were the most sensitive method for detecting hematite.

The FORC distribution could be more sensitive in detecting mixtures from changes in coercivity distribution, but the coercivity distributions appear very similar for all mixtures, especially for hematite concentration of 85 wt per cent or less, which is similar to what was found by Carvallo & Muxworthy (2006). Focusing on the coercivity profile in low fields show a distinct difference from pure magnetite with the initial addition of 10 wt per cent hematite with the appearance of a shoulder in the coercivity spectra under 22 mT, although the peak in the coercivity distribution remains the same as

pure magnetite for hematite concentrations ≤ 80 wt per cent (Fig. S3). Thus, the higher coercivity component is overwhelmed by the magnetite contribution, and cannot be detected by FORC analysis until 80 wt per cent concentration or higher (Fig. S4).

A two end-member PCA, noted a trend in the PCA scores with a significant change at concentrations of *ca.* 90 wt per cent or higher, which is a similar concentration as was found in the earlier studies. This holds, even though the magnetic properties of hematite in Frank & Nowaczyk (2008) and Carvallo & Muxworthy (2006) were not exactly the same as in this study. The method, however, fails at properly separating the high coercivity end-member as seen from the generated FORC for EM2. One source of error can arise from the fact that the FORC method assumes the magnetization is saturated, which is not the case for high coercivity hematite.

A general comment on the ability of any magnetic method to delineate between different ferromagnetic minerals will be dependent on how strongly different the magnetic properties are among mineral phases. The intensity of the saturation magnetization will be a key factor, because if one phase has M_s much stronger than any other phase it will dominate any induced magnetic measurement. Difference in coercivity and the narrowness of the coercivity distribution of the individual minerals will also play an important role. Two earlier study Robertson & France (1994) and Hejda *et al.* (1994) evaluated magnetic properties of magnetite–hematite mixtures, in which the hematite component was larger than the magnetite concentration. Hejda *et al.* (1994) examined hysteresis curves of hematite and magnetic mixtures with hematite concentration was between 1.67 and 500 times larger than the magnetite concentration, and found that magnetite contributed to the hysteresis behaviour in low field. In their case, however, the hysteresis properties did not appear additive, which led them to speculate on the role of interaction between the ferrimagnetic and antiferromagnetic phases played an important role without providing any detailed explanation. Egli (2004) demonstrated how magnetite with different coercivities can be unmixed from their behaviour during alternating demagnetization. Therefore, key to any separation is the whether the magnetic properties of the different contributions are distinct and magnetic interactions are not affecting the bulk properties of the materials.

In summary, the magnetic techniques and parameters that are used standardly to identify hematite, that is M_{RS}/M_S , B_{CR}/B_C , S -ratio or HIRM, are only useful when the hematite concentration is >90 wt per cent to 95 wt per cent. Acquisition curves of IRM or DCD curves, on the other hand, will not be saturated when the hematite concentration is around 30 wt per cent, but it often requires higher concentrations until the lack of saturation is obvious and larger than any uncertainty in the measurement. The additional use of PCA of FORC results may be useful in identifying the contribution from a secondary phase, but the method also has limitations. A combination of more than one method, however, can lead to a better discrimination of hematite when it occurs together with magnetite and/or maghemite. In the future addition of different magnetic measurements in a PCA, for example IRM acquisition, Curie/Néel temperature, could lead to a more robust separation of phases.

The results from this work once again highlight the difficulties in identifying hematite when it occurs together with magnetite or maghemite. The ability to better distinguish between these phases can be important in palaeomagnetic and environmental magnetic studies. For palaeomagnetism identification of the presence of magnetic iron oxides can be important for understanding when a rock has obtained its primary or secondary magnetization. Hematite occurs often as a secondary phase in sediments, and its presence indicates that a secondary magnetization exists. The timing of the

secondary magnetization, however, may be at the time of the rock lithification (e.g. Channell *et al.* 1982) or later in a rock's geological history. The presence of hematite can also provide information on chemical alteration in rocks. In environmental studies identification of hematite helps in discerning changes in redox state. A further application is the area of material sciences in characterizing the purity of synthesized iron oxide particles. Many applications require a material with high saturation magnetization and superparamagnetic properties. Surface oxidation of these very fine particles can greatly affect their magnetic properties and therefore their usefulness in application.

5 CONCLUSION

In this study, we demonstrate that PCA based on FORC is not successful in discriminating of the presence of hematite in the presence of magnetite, and FORC measurements require a significant concentration in order to see a high coercivity component. Although a hematite concentration of at least >30 wt per cent is needed to have a first indication that a high coercivity phase is present, a higher concentration is often required to have an undisputable indication. For this reason, full IRM or backfield IRM acquisition is better than using bulk hysteresis properties or standard S -ratio or HIRM. The results from this study highlight the difficulty in discerning hematite when it is found together with magnetite, and they serve as a caveat that hematite may make up a significant portion of iron oxides in geological material, even though they do not contribute significantly to the bulk magnetic properties. This is especially a point that must be remembered when identifying mineral phases in relationship to environmental or palaeomagnetic studies.

ACKNOWLEDGEMENTS

The authors would like to thank Stefan Beetschen for his help with samples preparation instrumentation. We also thank an anonymous reviewer, R. Egli and E. Petrovsky for their critical comments, which helped improve the manuscript. This study was supported by the National Nature Science Foundation of China (41604121), Hubei Provincial Natural Science Foundation, China (2017CFB611) and China Scholarship Council (201706410009).

REFERENCES

- Ahmadzadeh, M., Romero, C. & McCloy, J., 2018. Magnetic analysis of commercial hematite, magnetite, and their mixtures, *AIP Adv.*, **8**(5), 056807, doi:10.1063/1.5006474.
- Bloemendal, J., Lamb, B. & King, J., 1988. Paleoenvironmental implications of rock-magnetic properties of late quaternary sediment cores from the eastern equatorial atlantic, *Paleoceanography*, **3**(1), 61–87.
- Carvallo, C. & Muxworthy, A., 2006. Low-temperature first-order reversal curve (FORC) diagrams for synthetic and natural samples, *Geochem. Geophys. Geosyst.*, **7**(9), doi:10.1029/2006GC001299.
- Channell, J.E.T., Freeman, R., Heller, F. & Lowrie, W., 1982. Timing of diagenetic haematite growth in red pelagic limestones from Gubbio (Italy), *Earth planet. Sci. Lett.*, **58**(2), 189–201.
- Dunlop, D.J., 2002. Theory and application of the day plot (M_{RS}/M_S versus H_{cr}/H_c) 1. Theoretical curves and tests using titanomagnetite data, *J. geophys. Res.: Solid Earth*, **107**(B3), 2056, doi:10.1029/2001JB000486.
- Dunlop, D.J. & Carter-Stiglitz, B., 2006. Day plots of mixtures of superparamagnetic, single-domain, pseudosingle-domain, and multidomain magnetites, *J. geophys. Res.: Solid Earth*, **111**, B12S09, doi:10.1029/2006JB004499.

- Dunlop, D.J. & Özdemir, Ö., 1997. *Rock Magnetism: Fundamentals and Frontiers*, Cambridge University Press.
- Egli, R., 2004. Characterization of individual rock magnetic components by analysis of remanence curves. 3. Bacterial magnetite and natural processes in lakes, *Phys. Chem. Earth*, **29**, 869–884.
- Egli, R., 2013. VARIFORC: an optimized protocol for calculating non-regular first-order reversal curve (FORC) diagrams, *Global Planet. Change*, **110**(6), 302–320.
- Egli, R., Chen, A.P., Winklhofer, M., Kodama, K.P. & Horng, C.-S., 2010. Detection of noninteracting single domain particles using first-order reversal curve diagrams, *Geochem. Geophys. Geosyst.*, **11**(1), Q01Z11, doi:10.1029/2009GC002916.
- Frank, U. & Nowaczyk, N.R., 2008. Mineral magnetic properties of artificial samples systematically mixed from haematite and magnetite, *Geophys. J. Int.*, **175**(2), 449–461.
- Harrison, R.J. & Feinberg, J.M., 2008. FORCinel: an improved algorithm for calculating first-order reversal curve distributions using locally weighted regression smoothing, *Geochem. Geophys. Geosyst.*, **9**(5), Q05016, doi:10.1029/2008GC001987.
- Harrison, R.J., Muraszko, J., Heslop, D., Lascu, I., Muxworthy, A.R. & Roberts, A.P., 2018. An improved algorithm for unmixing first-order reversal curve diagrams using principal component analysis, *Geochem. Geophys. Geosyst.*, **19**, 1595–1610.
- Hejda, P., Kapicka, A., Petrovsky, E. & Sjöberg, B.A., 1994. Analysis of hysteresis curves of samples with magnetite and hematite grains, *IEEE Trans. Magn.*, **30**(2), 881–883.
- Heslop, D., 2015. Numerical strategies for magnetic mineral unmixing, *Earth Sci. Rev.*, **150**, 256–284.
- Heslop, D., Dekkers, M.J., Kruiver, P.P. & Van Oorschot, I.H.M., 2002. Analysis of isothermal remanent magnetization acquisition curves using the expectation-maximization algorithm, *Geophys. J. Int.*, **148**(1), 58–64.
- Heslop, D. & Dillon, M., 2007. Unmixing magnetic remanence curves without a priori knowledge, *Geophys. J. Int.*, **170**(2), 556–566.
- Heslop, D. & Roberts, A.P., 2012a. Estimating best fit binary mixing lines in the Day plot, *J. geophys. Res.: Solid Earth*, **117**, B01101, doi:10.1029/2011JB008787.
- Heslop, D. & Roberts, A.P., 2012b. A method for unmixing magnetic hysteresis loops, *J. geophys. Res.: Solid Earth*, **117**, B03103, doi:10.1029/2011JB008859.
- Heslop, D., Roberts, A.P. & Chang, L., 2014. Characterizing magnetofossils from first-order reversal curve (FORC) central ridge signatures, *Geochem. Geophys. Geosyst.*, **15**(6), 2170–2179.
- King, J.W. & Channell, J.E.T., 1991. Sedimentary magnetism, environmental magnetism, and magnetostratigraphy, *Rev. Geophys.*, **29**, 358–370.
- Kruiver, P.P., Dekkers, M.J. & Heslop, D., 2001. Quantification of magnetic coercivity components by the analysis of acquisition curves of isothermal remanent magnetisation, *Earth planet. Sci. Lett.*, **189**, 269–276.
- Kumari, M., Widdrat, M., Tompa, E. & Uebe, R., 2014. Distinguishing magnetic particle size of iron oxide nanoparticles with first-order reversal curves, *J. appl. Phys.*, **116**(12), 1222–1244.
- Lagroix, F. & Guyodo, Y., 2017. A new tool for separating the magnetic mineralogy of complex mineral assemblages from low temperature magnetic behavior, *Front. Earth Sci.*, **5**, 61, doi:10.33389/feart.2017.00061.
- Lascu, I., Banerjee, S.K. & Berquó, T.S., 2010. Quantifying the concentration of ferrimagnetic particles in sediments using rock magnetic methods, *Geochem. Geophys. Geosyst.*, **11**(8), Q08Z19, doi:10.1029/2010GC003182.
- Lascu, I., Harrison, R.J., Li, Y., Muraszko, J.R., Channell, J.E.T., Piotrowski, A.M. & Hodell, D.A., 2015. Magnetic unmixing of first-order reversal curve diagrams using principal component analysis, *Geochem. Geophys. Geosyst.*, **16**(9), 2900–2915.
- Liu, Q., Banerjee, S.K., Jackson, M.J., Zhu, R. & Pan, Y., 2002. A new method in mineral magnetism for the separation of weak antiferromagnetic signal from a strong ferrimagnetic background, *Geophys. Res. Lett.*, **29**(12), 1565, doi:10.1029/2002GL014699.
- Lohße, A. *et al.*, 2016. Overproduction of magnetosomes by genomic amplification of biosynthetic gene clusters in a magnetotactic bacterium, *Appl. Environ. Microbiol.*, **82**(10), 3032–3041.
- Ludwig, P., Egli, R., Bishop, S., Chernenko, V., Frederichs, T., Rugel, G., Merchel, S. & Orgeira, M.J., 2013. Characterization of primary and secondary magnetite in marine sediment by combining chemical and magnetic unmixing techniques, *Global Planet. Change*, **110**(11), 321–339.
- Martin-Hernandez, F. & Hirt, A.M., 2013. Evidence for weak ferromagnetic moment within the basal plane of hematite natural crystals at low-temperature, *Geochem. Geophys. Geosyst.*, **14**(10), 4444–4457.
- Mayergoz, I.D., 1986. Mathematical models of hysteresis, *IEEE Trans. Magn.*, **22**(5), 603–608.
- Muxworthy, A., King, J.G. & Heslop, D., 2005. Assessing the ability of first-order reversal curve (FORC) diagrams to unravel complex magnetic signals, *J. geophys. Res. Atmos.*, **110**, B01105, doi:10.1029/2004JB003195.
- Muxworthy, A., Williams, W. & Virdee, D., 2003. Effect of magnetostatic interactions on the hysteresis parameters of single-domain and pseudo-single-domain grains, *J. geophys. Res.: Solid Earth*, **108**(B11), 2517, doi:10.1029/2003JB002588.
- Parry, L.G., 1982. Magnetization of immobilized particle dispersion with two distinct particle sizes, *Phys. Earth planet. Inter.*, **28**(3), 230–241.
- Pike, C.R., Roberts, A.P. & Verosub, K.L., 1999. Characterizing interactions in fine magnetic particle systems using first order reversal curves, *J. appl. Phys.*, **85**(9), 6660–6667.
- Pike, C.R., Roberts, A.P. & Verosub, K.L., 2001. First-order reversal curve diagrams and thermal relaxation effects in magnetic particles, *Geophys. J. R. astr. Soc.*, **145**(3), 721–730.
- Roberts, A.P., Cui, Y. & Verosub, K.L., 1995. Wasp-waisted hysteresis loops: Mineral magnetic characteristics and discrimination of components in mixed magnetic systems, *J. geophys. Res.: Solid Earth*, **100**(B9), 17909–17924.
- Roberts, A.P., Pike, C.R. & Verosub, K.L., 2000. First-order reversal curve diagrams: a new tool for characterizing the magnetic properties of natural samples, *J. geophys. Res.: Solid Earth*, **105**(B12), 28461–28475.
- Robertson, D.J. & France, D.E., 1994. Discrimination of remanence-carrying minerals in mixtures, using isothermal remanent magnetisation acquisition curves, *Phys. Earth planet. Inter.*, **82**(3), 223–234.
- Thompson, R. & Oldfield, F., 1986. *Environmental Magnetism*, Allen & Unwin.
- Winklhofer, M. & Zimanyi, G.T., 2006. Extracting the intrinsic switching field distribution in perpendicular media: A comparative analysis, *J. appl. Phys.*, **99**(8), 08E710, doi:10.1063/1.2176598.

SUPPORTING INFORMATION

Supplementary data are available at *GJI* online.

Figure S1. Magnetic hysteresis loops for all samples with different magnetite/hematite ratios.

Figure S2. Variation of B_C , B_{CR} , IRM , M_S , M_{RS} and M_{RS}/M_R as a function of hematite concentration.

Figure S3. Horizontal profile of the FORC diagram along the dashed line in Fig. 5.

Figure S4. FORC diagram of samples Mt_Hm_80, Mt_Hm_90, Mt_Hm_95, showing the coercivity distribution between 100 and 700 mT. FORC diagrams were processed with the MatLAB code of Winklhofer & Zimanyi (2006).

Table S1. Error estimation for S -ratio, HIRM and B_{CR}/B_C .

Please note: Oxford University Press are not responsible for the content or functionality of any supporting materials supplied by the authors. Any queries (other than missing material) should be directed to the corresponding author for the paper.